
Article:
Cobo, C. C., Arran, C. orcid.org/0000-0002-8644-8118, Bourgeois, N. et al. (20 more authors) (2024) Target sensitivity study of density transition-injected electrons in laser wakefield accelerators. Physical Review Accelerators and Beams. 111301. ISSN 2469-9888

https://doi.org/10.1103/PhysRevAccelBeams.27.111301

Target sensitivity study of density transition-injected electrons in laser wakefield accelerators

C. C. Cobo,[1,*] C. Arran,[1] N. Bourgeois,[2] L. Calvin,[3] J. Carderelli,[4] N. Cavanagh,[3] C. Colgan,[5] S. J. D. Dann,[2] R. Fitzgarrald,[4] E. Gerstmayr,[5,6] B. Kettle,[5] E. E. Los,[5] S. P. D. Mangles,[5] P. McKenna,[7] Z. Najmudin,[5] P. P. Rajeev,[2] C. P. Ridgers,[1] G. Sarri,[3] M. J. V. Streeter,[3] D. R. Symes,[2] A. G. R. Thomas,[4] R. Watt,[5] and C. D. Murphy[1,†]

[1]*York Plasma Institute, School of Physics, Engineering and Technology, University of York, York, YO10 5DD United Kingdom*

[2]*Central Laser Facility, STFC Rutherford Appleton Laboratory, Didcot OX11 0QX, United Kingdom*

[3]*School of Mathematics and Physics, Queen's University Belfast, Belfast BT7 1NN, United Kingdom*

[4]*Center for Ultrafast Optical Science, University of Michigan, Ann Arbor, Michigan 48109-2099, USA*

[5]*The John Adams Institute for Accelerator Science, Imperial College London, London SW7 2AZ, United Kingdom*

[6]*Stanford PULSE Institute, SLAC National Accelerator Laboratory, Menlo Park, California 94025, USA*

[7]*Department of Physics, SUPA, University of Strathclyde, Glasgow, G4 0NG, United Kingdom*

(Received 14 June 2024; accepted 12 November 2024; published 26 November 2024)

While plasma-based accelerators have the potential to positively impact a broad range of research topics, a route to application will only be possible through improved understanding of their stability. We present experimental results of a laser wakefield accelerator in the nonlinear regime in a helium gas jet target with a density transition produced by a razor blade in the flow. Modifications to the target setup are correlated with variations in the plasma density profile diagnosed via interferometry and the shot-to-shot variations of the density profile for nominally equal conditions are characterized. Through an in-depth sensitivity study using particle-in-cell simulations, the effects of changes in the plasma density profile on the accelerated electron beams are investigated. The results suggest that blade motion is more detrimental to stability than gas pressure fluctuations, and that early focusing of the laser may reduce the deleterious effects of such density fluctuations.

DOI: 10.1103/PhysRevAccelBeams.27.111301

I. INTRODUCTION

Laser wakefield acceleration (LWFA) is capable of generating gigaelectronvolt-energy electrons in centimeter-scale interaction lengths via the ponderomotive excitation of a relativistic plasma wave by a high intensity laser [1]. These accelerators constitute promising compact sources of relativistic electrons, which could drive impact in areas ranging from laboratory astrophysics [2] to biological imaging [3]. Improvements in technology and understanding of LWFA have enabled the demonstration of electron beams with few percent energy spread via self-injection in the bubble regime [4–6], nanocoulomb-class electron bunches via ionization injection [7], and energy gains up to 8 GeV in a 20 cm waveguide [8]. These characteristics, combined with the femtosecond duration of LWFA electron bunches [9,10], have led to extensive research into applications of LWFA such as in fundamental physics investigations of strong-field quantum electrodynamics [2], and as sources for gamma rays [11], electron diffraction [12] and bright x-rays through betatron oscillations [3,13], Compton scattering [14], and free-electron lasing [15]. However, improvements in the stability, reliability, and robustness of electron beam parameters are still required to develop these applications beyond proof of principle [16,17]. In order to obtain the required stable operation, it is necessary to characterize all sources of experimental fluctuation.

In LWFA, the electron injection and acceleration dynamics are determined by the nonlinear evolution of the laser driver as it traverses the plasma. Thus small fluctuations in the experimental conditions can cause significant shot-to-shot variations of the electron beam parameters. The need

*Contact author: c.cobo@imperial.ac.uk
Present address: The John Adams Institute for Accelerator Science, Imperial College London, London SW7 2AZ, United Kingdom.
†Contact author: chris.murphy@york.ac.uk

to maintain good density stability to minimize shot-to-shot fluctuations of electron beam energy and charge has been demonstrated for self-injection in a steady-state gas cell [18]. Similarly, nonuniformities in the density profile have been shown to cause variations in electron energy gain [19]. Controlled mechanisms of injection have demonstrated improved short-term stability compared to self-injection through the use of colliding laser pulses [20] or plasma density tailoring [21]. Recently, long-term stability over $\sim 100,000$ shots at high repetition rate was demonstrated through high statistics experimental approaches using ionization injection. These have shown strong correlations of electron beam parameters with fluctuations of the laser energy [22] and plasma density [23] and conclude that stable ionization injection requires tight constraints on the reproducibility of the interaction parameters.

Density down ramp injection is a mechanism of controlled injection, which could improve electron beam stability. By avoiding very high laser intensities and target densities and thus limiting self-injection, the dependence of the electron trapping process on the laser-plasma coupling should weaken. Localization of the injection process can be achieved by the sudden increase of the plasma wavelength $\lambda_p \propto n_e^{-1/2}$ in a sharp density transition, with length scale $L < \lambda_p$ [24], or via a locally reduced nonlinear wave-breaking threshold on a long scale-length density ramp, $L \gg \lambda_p$ [25]. In the latter, the lengthening of the plasma wavelength within the decreasing density gradient requires the phase velocity of the plasma wave v_{ph} to be slower than the group velocity of the laser v_{gl}. This local decrease of v_{ph} in the ramp causes the relaxation of the injection threshold, which requires electron velocities $v_e > v_{\mathrm{ph}}$.

Density transition injection has been realized experimentally by introducing a razor blade into a supersonic gas jet target [26], producing stable and tunable low energy spread electron beams [27,28]. The density and length scale of the shock produced by this setup have been shown to vary with gas pressure, blade position, and height of the interaction above the blade [29]. Extensive simulation work has studied the dependence of electron beam parameters on the transition length ranging from the sharp to the long scale regime [30], the influence of ramp steepness on electron beam quality [31], and the effect of transition length, height, and laser energy on electron beam parameters [32,33]. However, the density profile in experiments fluctuates over time and between shots, thereby reducing the stability of the electron beam charge and energy. There have been no dedicated investigations of these fluctuations, which include coupled variations of the peak and plateau densities, as well as changes to the down ramp position relative to the laser focus. Studies of the source of these fluctuations, which indicate the robustness of the density-tailoring technique, are similarly lacking.

In this work, we present experimental results of parameter scans used to tailor the target density profile in a laser wakefield accelerator and optimize density transition-injected electron beams using a supersonic gas flow target interrupted by a blade. The shot-to-shot fluctuations of the target density profile are measured experimentally, together with the electron beam charge and energy fluctuations as motivation for the target sensitivity study. The sensitivity of the accelerated electron beams to the experimentally measured density fluctuations are understood through particle-in-cell simulations. These investigations reveal the relative importance of different aspects of the density profile and the limitations to the density-tailoring setup.

II. EXPERIMENT

The experiment was conducted using the Gemini laser system at the Central Laser Facility in the United Kingdom (see [34] for further details of the setup). A GeV-scale LWFA was driven by laser pulses with energy (6.6 ± 0.5) J, pulse duration $\approx$50 fs, and central wavelength 800 nm. An $f/40$ off-axis parabolic mirror focused the pulses to a $(50 \pm 2) \times (45 \pm 2)$ μm spot onto a helium supersonic gas jet target produced by a gas nozzle with a diameter of 15 mm. A razor blade was placed in the gas flow to produce a shock front along the laser axis that comprised a decreasing density ramp for density transition injection [26]. The electron density profile along the laser-generated channel was measured using interferometry with a short-pulse transverse probe beam. The target setup and a representative interferometry measurement of the electron density profile are shown in Fig. 1. The density profile is characterized by the plateau density n, peak density N, and ramp position z_{ramp} as defined in Fig. 1(b). The same razor blade was used to produce the density ramp in all shots. No damage to the blade was noted, and no decline of the density profile quality or stability over time was measured.

The density transition length is measured to be of the order 1 mm, which is at least an order of magnitude higher than expected for the setup and pressures used [26–29]. This overestimate can be attributed to the assumption of

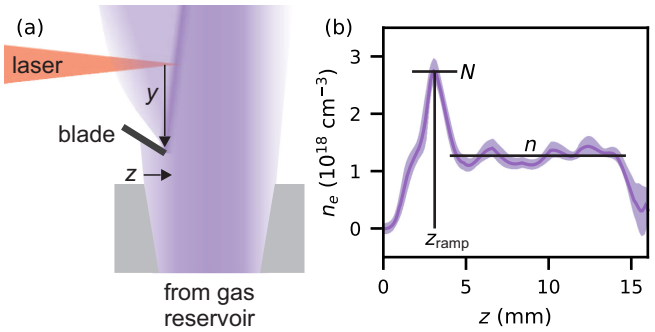

FIG. 1. (a) Schematic diagram of the target used in the experiment. (b) Representative electron density profile along the direction of laser propagation retrieved from interferometry measurements; the shaded region represents the experimental uncertainties.

cylindrical symmetry in the Abel inversion and imperfect alignment of the probe beam perpendicular to the shock. Therefore, despite being a useful diagnostic for the electron density present in the peak and plateau, the shape and extent of the density ramp is not considered to be accurate and measurements of the ramp length are not discussed.

A. Experimental motivation

While there is a sound reason to believe that introducing a density transition to a gas jet would decrease the shot-to-shot fluctuations in accelerated electron parameters, such a transition may also introduce an additional source of variability. We consider such an experiment, where the beam fluctuations were significant, in order to motivate the simulations presented in this study. Forty four shots were taken at nominally identical initial conditions, at backing pressure $P = 70$ bar, blade coverage $z = 0.5$ mm, and with the laser axis $y = 13$ mm above the blade and 18 mm above the gas nozzle. This resulted in plateau densities $n = (0.86 \pm 0.07)\,\mathrm{cm}^{-3}$ and peak densities $N = (1.8 \pm 0.2)\,\mathrm{cm}^{-3}$, where the uncertainties are 1σ. The peak and plateau densities were weakly correlated, with correlation coefficient $r = 0.3$.

The electron energy spectra were measured using an electron spectrometer comprising a magnetic dipole and two scintillating Lanex screens. The images on the screen were energy-calibrated by numerical tracking of electron trajectories in the magnetic field and detected electrons with energies between 0.3 and 2.5 GeV. Automated edge detection was employed on the electron spectra in divergence-energy space to measure the maximum electron beam energy for every shot. The total charge was measured by integrating the signal in the electron spectrometer.

The distributions of injected charge and maximum electron beam energy are presented in Fig. 2. The maximum electron beam energy was observed to fluctuate by $\pm 18\%$ ($1\sigma = 150$ MeV), while the injected charge varied by $> 40\%$ at 1σ. The observed fluctuations in electron beam parameters are more severe than expected from the use of controlled injection via longitudinal density tailoring [26–28]. Gaining insights into these measurements requires improved understanding of the effects of target fluctuations relevant to the experiment.

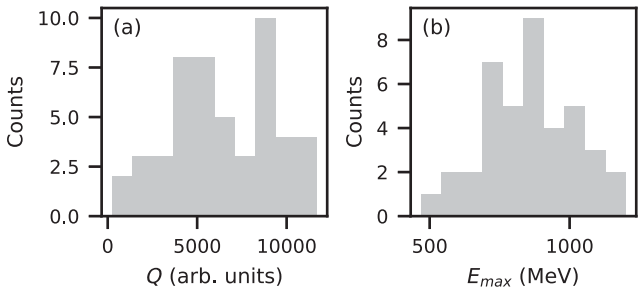

FIG. 2. Experimental data of the accelerated electron beams from 44 shots at the same nominal initial conditions. Distributions of (a) injected charge and (b) maximum electron beam energy.

B. Target density profile scans

To investigate the dependence of the target density profile on input target parameters, the backing pressure P of the gas jet and the vertical y and horizontal z positions of the blade were scanned, with three to five shots taken at each set of initial conditions. The position of the gas jet and laser axis were fixed. The gas pressure was varied between 50 and 100 bar; the blade y between 2 and 16 mm below the laser axis and the blade z between 0 and 11 mm coverage of the gas jet.

Figure 3 shows the plateau density n, peak density N, and ramp position z_{ramp} as a function of input target parameters for representative parameter scans. Figures 3(a) and 3(b) show that changes in the backing pressure between 55 and 95 bar result in approximately linear variations of both the peak and plateau densities, maintaining a constant peak: plateau ratio of 2.4 ± 0.3. The correlation coefficient between peak and plateau densities is $r = 0.95$ for the pressure scan. By contrast, changes to the blade position break the correlation between peak and plateau density, as shown in Figs. 3(d) and 3(e) for a scan of vertical blade position. Increasing the blade y causes a decrease in the

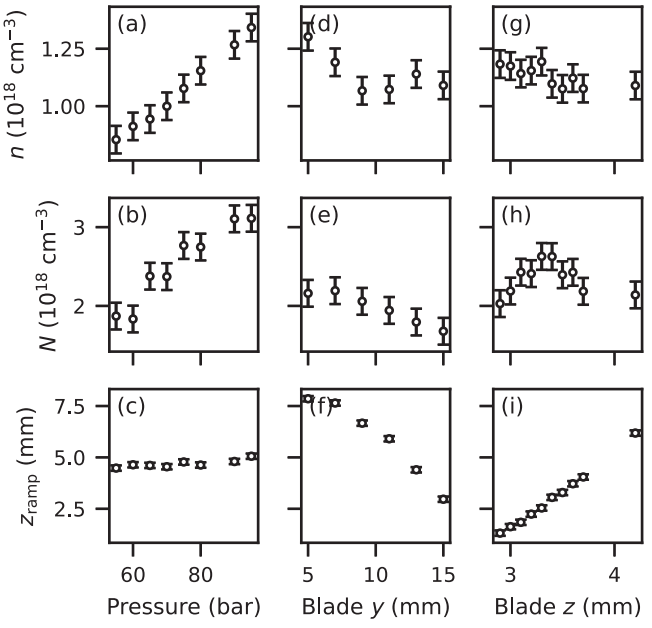

FIG. 3. The left column shows the response of (a) plateau density, (b) peak density, and (c) ramp position as a function of backing pressure. (d)–(f) and (g)–(i) show the same parameters for blade height and blade coverage, respectively. Each point is the average of three to five shots and the error bars represent the shot-to-shot fluctuations ($\pm 1\langle\sigma\rangle$) discussed in Sec. II C. For the pressure scan, $y = 6.5$ mm and $z = 3.2$ mm. For the blade y scan, $P = 100$ bar and $z = 3.5$ mm.

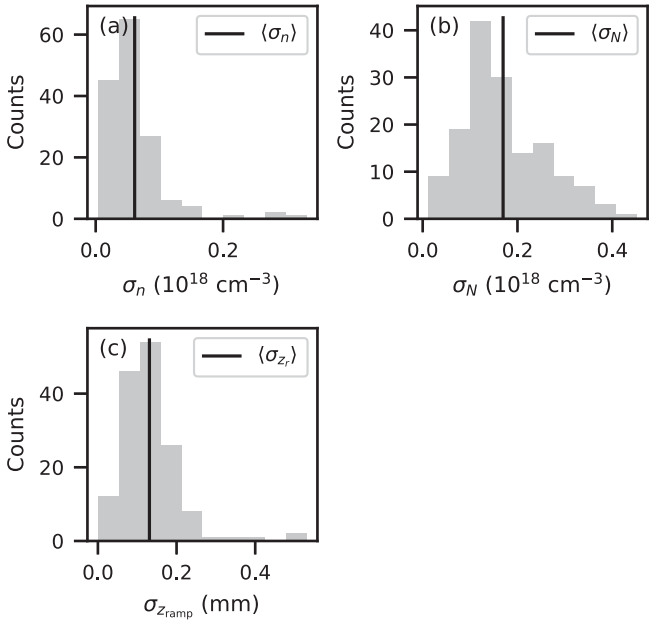

FIG. 4. Shot-to-shot density fluctuations of (a) plateau density, (b) peak density, and (c) ramp position. The gray histogram represents the distribution of sample standard deviations σ calculated for samples comprising three to five shots at the same nominal initial conditions. The black line denotes the mean of the distribution, which represents the population standard deviation $\langle\sigma\rangle$.

peak density with an anomalous result for the lowest blade position; this is likely due to the curvature of the shock and so will be disregarded. The plateau density remains approximately constant; the correlation coefficient between peak and plateau densities is $r = 0.38$ for this scan (disregarding the anomalous result). Changing the horizontal position of the blade again has little effect on the plateau density but an erratic effect on the peak density, as shown in Figs. 3(g) and 3(h). A negative correlation is observed when the blade coverage is under 3 mm, but this trend inverts for larger blade coverages ($r = 0.01$). The correlated peak and plateau densities are indicative of a variation in gas backing pressure, while a lack of correlation between the densities implies motion of the blade in the gas.

The position of the density down ramp is found to be strongly affected by the position of the blade in the gas jet, as shown in Figs. 3(f) and 3(i). The density ramp is observed to move outward as the blade is moved farther below the laser axis, representing an outward shock. This is representative of a gentle intercepting shock that develops farther from the blade [29], rather than the sharp bow shock that forms near the blade. The ramp position is most sensitive to longitudinal motion of the blade, varying at a rate (3.7 ± 0.8) mm mm^{-1}. Figure 3(c) shows that the gas pressure has a weak effect on the ramp position but still comparable to or larger than the shot-to-shot fluctuations for pressure variations of order 10 bar. Therefore, gas pressure and blade position are the main sources of experimental fluctuation.

TABLE I. Measured shot-to-shot fluctuations of the density parameters. The third column presents the fluctuations as a percentage of the baseline simulation parameters from Sec. III; the ramp position is given as a percentage of the laser's Rayleigh range.

Parameter	Absolute $2\langle\sigma\rangle$	Relative $2\langle\sigma\rangle$ (%)
Plateau density n	0.12×10^{18} cm^{-3}	10
Peak density N	0.34×10^{18} cm^{-3}	12
Ramp position z_{ramp}	260 μm	17

C. Shot-to-shot density fluctuations

A measure of the shot-to-shot fluctuations of the density characteristics was obtained by taking repeat shots at the same nominal initial conditions. The distribution of the density characteristics has a spread characterized by the sample standard deviation σ, which is an estimator of the fluctuations. By measuring σ for every set of shots at the same initial conditions, it is possible to build a distribution of the measured fluctuations, as shown in Fig. 4. Here there are 145 samples comprising 628 shots taken over 2 days. The average of the set of standard deviations, $\langle\sigma\rangle$, is the population standard deviation, which is expected to accurately represent the spread of possible density values obtained with the same setup, assuming that the fluctuations are independent of the absolute density values. This assumption is valid for the range of density profiles used in the experiment, as each measured sample standard deviation is weakly correlated with the sample mean for the plateau density ($r = 0.03$) and peak density ($r = 0.24$). Thus the shot-to-shot fluctuations can be characterized by the spreads $2\langle\sigma\rangle$, which represent 68% of the possible density values obtained and are summarized in Table I.

Fluctuations in the peak density are 2.8 times higher than those in the plateau density. Fluctuations in the ramp position are ∼260 μm, which is small compared to the focusing geometry of the laser (Rayleigh range > 4 mm). The measured density fluctuations are used to inform the particle-in-cell simulations presented in Sec. III.

III. SIMULATIONS

Two-dimensional simulations of density transition injection were performed using the particle-in-cell code EPOCH [35] to investigate the sensitivity of the electron beam charge and maximum energy to fluctuations in the peak and plateau densities and ramp position. The simulations were not designed to model the full experimental results but to systematically study the fluctuations of electron beam parameters. Therefore, the target fluctuations measured

from the experiment were applied to a simplified density profile in this numerical study.

The target comprised a preionized plasma with a 360 μm rising edge to a peak density N, followed by a down ramp onto a plateau region at density n. To be computationally tractable, only the injection and initial acceleration dynamics are considered; the total propagation distance was 1.2 mm, with the electron spectrum characterized after 4 ps. Since the charge of the bunch is primarily set by the injection, we expect a shorter simulation to give a good indication of the charge at the end of a longer accelerator. After injection, the energy gained by the electrons is determined by their phase, the length of the accelerator and the accelerating field (which is, to first order, set by the plateau plasma density). Thus the variation in electron beam energy prior to dephasing can be assessed by the energy a shorter distance after injection.

The down ramp had a $\tanh[(z-z_r)/w)]$ form with characteristic length $w = 20$ μm. w corresponds to an effective total density transition length ≈80 μm, which is in the gentle ramp regime for a plasma wavelength $\lambda_p \approx 25$ μm and is consistent with recent measurements [27,28]. The density profile for the baseline simulation is shown in Fig. 5(a). The baseline (denoted by subscript 0) comprises a peak density $N_0 = 2.82 \times 10^{18}$ cm^{-3}, plateau density $n_0 = 1.2 \times 10^{18}$ cm^{-3} ($N_0/n_0 = k_0 = 2.35$), and vacuum laser focus at the middle of the down ramp, $z_{r0} = 400$. n_0 represents the average plateau density used in the experiment. The laser had Gaussian temporal and transverse profiles with 50 fs pulse duration and 46 μm diameter beam waist. The vacuum laser intensity was 2×10^{19} W cm^{-2}.

The simulations were performed with a window size 64 × 112 μm (longitudinal × transverse) with 4800 × 2800 cells and 8 particles per cell. Convergence tests suggest the injected charge and maximum electron energy to have an uncertainty $< 1\%$ with these parameters. Simulations performed with no down ramp at densities n_0 and N_0 show that a nonlinear wakefield is produced, but no self-injection occurs in the first wakefield period. Thus these simulations allow the study of the density transition injection dynamics.

Three sets of simulations were run, based on the experimentally measured trends of density characteristics with target inputs, each of which isolated one kind of density fluctuation. Simulation set I varied the peak density only, $n = n_0$; set II varied the plateau and peak densities at a constant ratio, $N/n = k_0$; set III varied the laser focus z_l relative to the position of the ramp. Within each set, four simulations were run at $\pm 1\langle\sigma\rangle$ and $\pm 2\langle\sigma\rangle$ away from the baseline relevant density parameter, where $2\langle\sigma\rangle$ represent the experimental shot-to-shot fluctuations in Table I. The deviations of injected charge from the baseline ΔQ and the deviations of maximum electron energy from the baseline $\Delta(E_{max})$ are calculated at the end of the simulation and given as a percentage of the baseline quantity. Only the electrons in the first wakefield period are considered. The electron energy spectra depict a sharp cutoff in a log-scale at both high and low energies. The high-energy cutoff E_{max} was identified by fitting the distribution function in energy to a $\tanh[(E - E_{max})/w_E]$ function, with the length scale of the step w_E taken as the measurement uncertainty. The simulations show that injection occurs only in the ramp. The baseline simulation accelerated 79 pC of electrons to a maximum energy of 68 MeV.

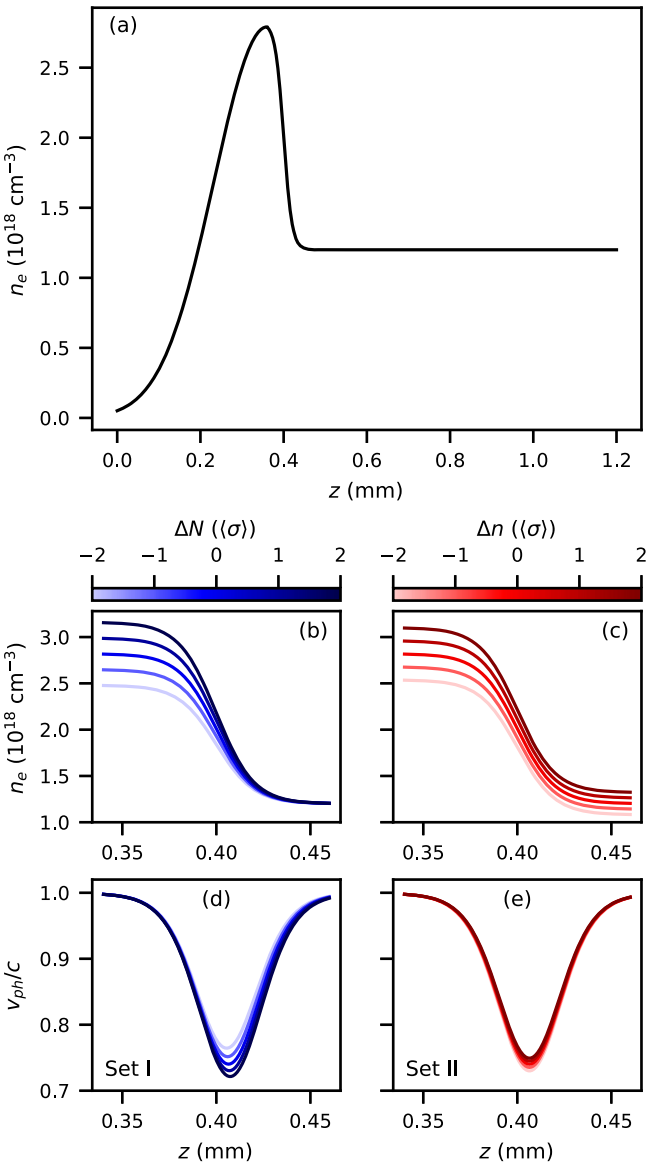

FIG. 5. (a) Baseline density profile for simulations. The density profile was varied as in (b) for simulation set I at constant plateau density and (c) for simulation set II with a constant N/n. (d), (e) Analytic phase velocity evolution caused by the density profiles in (b) and (c), respectively, during bubble elongation at $\zeta = -\lambda_p(n_e)$.

A. Sensitivity to absolute density

The density profiles used for simulation sets I and II are shown in Figs. 5(b) and 5(c), respectively. The wakefield phase velocity v_{ph} depends on the local plasma density as

$$v_{\mathrm{ph}} = v_{\mathrm{gl}}\left(1 + \frac{\zeta}{2n_e}\frac{\mathrm{d}n_e}{\mathrm{d}z}\right)^{-1}, \tag{1}$$

where $\zeta = z - v_{\mathrm{gl}}t$ and $v_{\mathrm{gl}} = c(1-\omega_p^2/\omega_0^2)^{1/2}$. Since the local decrease in v_{ph} relaxes the injection threshold, we may understand the injection dynamics through this. The evolution of v_{ph} at the back of the bubble is plotted in Figs. 5(d) and 5(e) for the simulated density ramps. The effect of the laser evolution on v_{ph} is neglected; while this also induces a change in v_{ph} (due to a changing a_0), we find this to be slow relative to the effect of the density gradient.

The charge and maximum energy deviations from the baseline caused by density fluctuations up to $2\langle\sigma\rangle$ are summarized in Fig. 6.

1. Injected charge

The injected charge is observed to increase with an increase in peak density in Fig. 6(a), both for constant and variable plateau densities. This indicates that the availability of electrons determines the injected charge. In addition, the decrease of the wakefield phase velocity in the ramp affects the injection process. When *only* the peak density changes, the injected charge increases by a factor of 2 more than when the peak and plateau densities are changed consistently. As depicted in Figs. 5(b) and 5(d), a higher peak density at a constant plateau represents a steeper density ramp, which causes the phase velocity of the wakefield to decrease by more and remain low over a longer region. This further enhances injection and indicates that, in this case, the peak density is the dominant contribution to charge variations. By contrast, coupled variations of peak and plateau densities cause a decrease in the wakefield phase velocity that is only weakly dependent on the densities used, as shown in Fig. 5(e).

2. Maximum electron beam energy

Simulation sets I and II display opposite trends of maximum electron beam energy with density in Fig. 6(b). For targets with a constant plateau density, the maximum electron energy is observed to decrease with increasing peak density. This may seem counter-intuitive since the accelerating field, to a first approximation, will be constant at constant plateau density, and it is in this region that acceleration takes place. While beam loading may partially explain the variation, the phase at which electrons are injected also plays a significant role.

The injected electron beams have a negative chirp, so the maximum electron beam energy is determined by the dynamics of the leading electrons, which are the first to

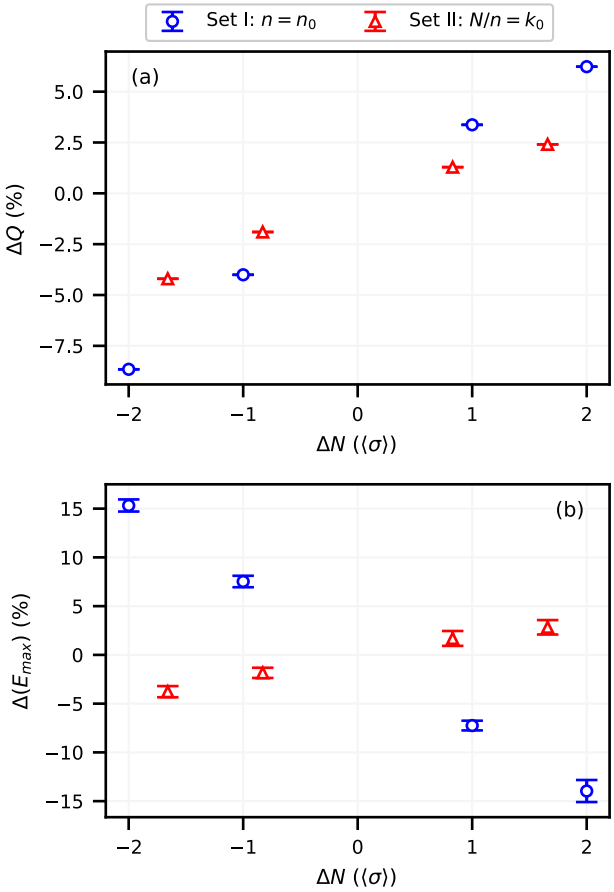

FIG. 6. Simulated absolute density fluctuations in a tailored plasma target after 1.2 mm. Deviation of (a) injected charge and (b) maximum electron beam energy from the baseline as a function of peak density fluctuations. The blue circles correspond to variations of the peak density at a constant plateau density (simulation set I), while the red triangles correspond to coupled variations of the peak and plateau densities at a constant ratio (simulation set II).

be injected. Increasing the peak density with a constant plateau density results in earlier injection, leading to electrons located at an advanced position ζ in the wake. This is because steeper ramps reach lower v_{ph} earlier in the interaction, as shown in Fig. 5(d). Injection also terminates later, resulting in a longer bunch duration. In ramps with a constant peak to plateau ratio, the opposite trend is expected, as Fig. 5(e) shows lower-density ramps causing v_{ph} to reach lower values at smaller z. However, as electrons inject from the back of the bubble, $\zeta = -\lambda_p(n_e)$, those injected at higher densities will be advanced in ζ on injection. The position of the leading electrons in the wakefield is depicted as the triangles in Fig. 7.

Figure 7(a) depicts the accelerating fields in simulation set I after 4 ps. The laser at $z = 1.19$ mm travels along z and drives a wakefield with longitudinal electric field E_z. The local maximum $-E_z$ in the inset coincides with the position of the leading high-energy electrons (triangles),

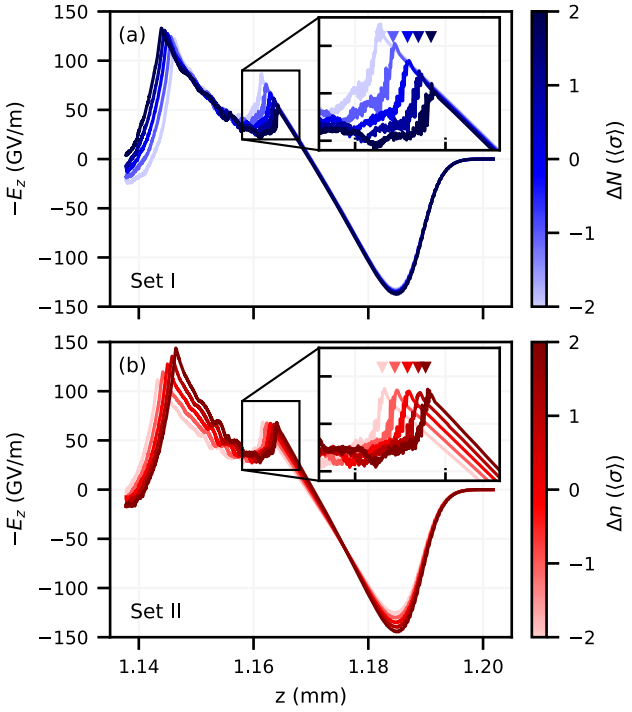

FIG. 7. Accelerating fields for simulations varying (a) only the peak density and (b) both the peak and plateau densities after 4 ps. The inset shows the accelerating fields in the vicinity of the leading high-energy electrons. The position of the leading electrons is shown by the triangles and coincides with the local maximum $-E_z$ for all simulations.

showing their separation in ζ as a result of the varying injection dynamics with peak density. The accelerating fields behind this point are suppressed by beam loading. In the vicinity of the leading electrons, the accelerating fields from the laser-driven wakefields decrease linearly with ζ. Therefore, the electrons injected from higher peak density targets, which are advanced in ζ, witness lower accelerating fields than those from lower density simulations. This positional effect compounds with beam loading, which is more significant for the higher charge injected with higher peak densities. Beam loading modifies the electric field at the back of the electron bunch, causing the effective plasma wave to appear longer for higher densities.

Conversely, coupled variations of peak and plateau densities result in an increasing trend of maximum electron beam energy with plasma density, with 3 times lower deviations. Figure 7(b) shows the accelerating fields in these simulations after 4 ps. The leading high-energy electrons (triangles) have a density-dependent ζ because the injection point moves forward at higher densities as a result of the shorter plasma wave. In contrast to simulation set I, the plateau density is different after injection, driving changes in the acceleration region. Increasing the density causes a simultaneous increase in the peak accelerating field and decrease in the plasma wavelength. Overall, the increase in peak field (due to higher plasma density) is coupled with the electrons being injected into an earlier phase of the wave (i.e., a lower field relative to the peak). These differences in the wavelength and amplitude of the laser-driven wakefield compensate for the different position of the leading electrons so that they witness more consistent accelerating fields as shown in Fig. 7(b). The result is more stable electron energies.

3. Stability

For simulation set I, the charge fluctuates by up to 8% while $\Delta(E_{\max})$ reaches 15% for 2σ density fluctuations. The results are consistent with previous studies [30,32], which report a reduction in mean electron energy as the density transition height is increased. For simulation set II, both the charge and the maximum electron beam energy fluctuate by up to 4% for 2σ input fluctuations.

The variations caused by changes in the peak density independent of the plateau cause 2 times larger deviations of the injected charge and 3 times larger deviations of the maximum electron beam energy. This is because the injection dynamics are sensitive to variations in $n_e^{-1}\mathrm{d}n_e/\mathrm{d}z$, and this in turn influences the acceleration dynamics through changes in the position of the electrons. Such variations were found experimentally to result from blade position fluctuations in the target in Sec. II C. It is expected that fluctuations in the ramp length would exacerbate this effect, as these also change the ramp steepness that strongly influences electron injection. By contrast, coupled variations of peak and plateau densities present improved stability. As these density fluctuations are associated with fluctuations in gas pressure, the results suggest that blade motion is more detrimental to stability than gas fluctuations. This indicates that a more robust method of producing the density ramp could improve the charge stability by a factor of 2 and the energy stability by a factor of 3.

B. Sensitivity to ramp position

Fluctuations of the down ramp position were simulated by moving the vacuum laser focus as depicted in Fig. 8(a),

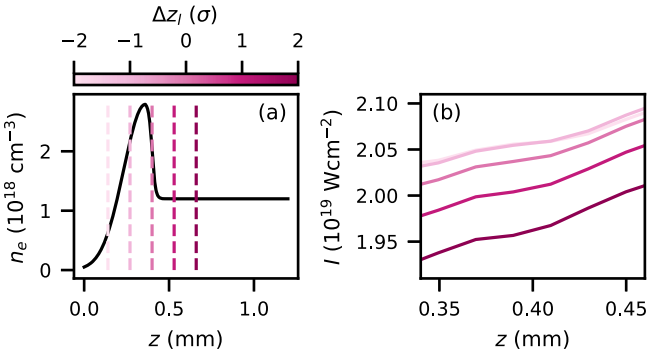

FIG. 8. (a) Density profiles used for simulation set III; the dashed lines show the position of vacuum laser focus. (b) Simulation results of the laser intensity evolution for the simulations in (a).

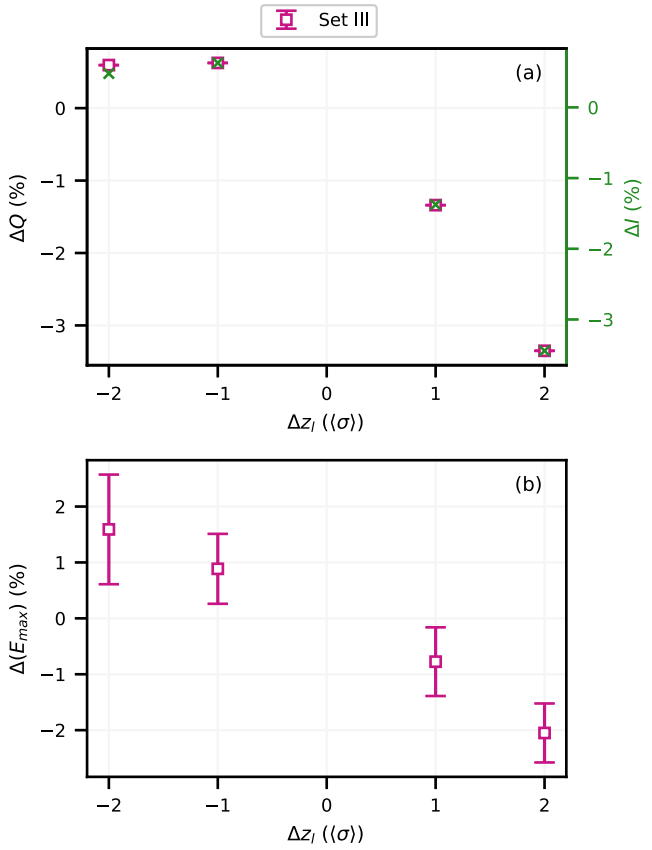

FIG. 9. Simulated ramp position fluctuations in a tailored plasma target after 1.2 mm. Deviation of (a) injected charge and (b) maximum electron energy from the baseline. $\Delta z_l = 0$ corresponds to the middle of the ramp aligned with the vacuum laser focus; positive Δz_l corresponds to a vacuum laser focus after the ramp. The green crosses in (a) depict the measured laser intensity deviations after 0.4 mm propagation.

where the laser intensity variations in the density ramp are shown in Fig. 8(b). The resulting charge and maximum electron beam energy deviations from the baseline simulation are shown in Fig. 9. Here, we define $\Delta z_l = -\Delta z_{\text{ramp}}$, such that motion of the ramp farther along the gas is equivalent to the laser focusing earlier.

The injected charge is observed to decrease when the ramp is positioned before vacuum laser focus. The evolution of the laser wavelength throughout the interaction is indistinguishable for simulations with different laser focus positions (deviations $< 0.002\%$ throughout). This implies that the laser energy depletion to the wakefield is comparable. However, the evolution of laser intensity varies more significantly, as a result of the different rates of self-focusing and self-compression for different initial laser spot sizes. This is depicted in Fig. 8(b) within the density transition. The intensity deviates by -4% and -2% from the baseline when the laser is set to focus 260 and 130 μm after the ramp, respectively. By contrast, setting the laser to focus before the ramp causes a 1% deviation in laser intensity, which is very weakly dependent on the magnitude of the translation between 130 and 260 μm. The laser intensity determines the electron velocities reached during oscillation in the wakefield, thereby influencing the number of particles that can inject. The observed charge deviations directly match the measured intensity variations in the ramp shown as the green crosses in Fig. 9(a), suggesting a linear dependence of injected charge to laser intensity, despite the complex dynamics involved. This implies that the injected charge will also be affected by fluctuations in laser energy.

Variations of the ramp position relative to the vacuum laser focus result in fluctuations of the maximum electron beam energy of $< 2\%$. The energy is observed to increase as the vacuum laser focus is moved before the ramp. This suggests that the increased laser-plasma coupling early in the interaction taking place for $\Delta z_l < 0$ dominates the initial acceleration dynamics simulated.

The simulations indicate that fluctuations of the ramp position relative to the laser focus are less detrimental to the injected charge and maximum electron beam energy than fluctuations of the absolute density. The results suggest that focusing the laser before the density transition is beneficial in terms of shot-to-shot charge stability, since the nonlinear dynamics will compensate an initial difference in intensity. However, the limits of this require further study.

IV. CONCLUSION

We present a practical study of density down ramp injection to improve the stability and applicability of LWFA electrons generated by this means. These types of sensitivity studies will help to define the required level of control and acceptable tolerances for a reliable accelerator. The shot-to-shot fluctuations of the plateau density, peak density, and down ramp position produced by a supersonic gas flow target interrupted by a blade were measured experimentally and reproduced in particle-in-cell simulations of the injection dynamics.

The sources of experimental density fluctuations were identified as the variable gas jet pressure and the variations of blade position. Changes in the longitudinal or vertical position of the blade result in independent variations of the peak and plateau densities, while density profile variations caused by changes in the gas jet backing pressure maintain a constant peak to plateau density ratio. Simulations reveal that decoupled variations of peak and plateau density drive larger fluctuations in charge and maximum energy. This strongly indicates that the fluctuations observed in our experimental data are more likely a result of a fluctuating blade rather than a variation in gas pressure. Therefore, a more robust method of producing the density ramp could improve the charge stability by a factor of 2 and the energy stability by a factor of 3. In addition to a more rigid obstruction to generate the down ramp, the simulations suggest that focusing the laser before the density structure

will likely reduce the fluctuations observed in the electron beams generated.

The results presented will enable future experimental campaigns to be designed to improve the stability of the accelerated electron beams through target design and laser focal position. This should allow the effect of other variations (e.g., due to laser parameters or the long acceleration region that was not simulated) to be more clearly observed. Such a systematic approach to improved stability of LWFA electron beams presents a path to the stable electron beams required for future applications in particle physics, medicine, and x-ray free electron laser applications.

ACKNOWLEDGMENTS

The project was conducted under the auspices of the University of York's Centre for Doctoral Training in Fusion Energy. This work was supported by the Engineering and Physical Sciences Research Council grant and EP/V044397/1 and US NSF Award No. 2108075. This project was undertaken on the Viking Cluster, which is a high performance compute facility provided by the University of York. The authors are grateful for computational support from the University of York's High Performance Computing Service, Viking, and the Research Computing Team.

[1] T. Tajima and J. M. Dawson, Laser electron accelerator, Phys. Rev. Lett. **43**, 267 (1979).

[2] J. M. Cole *et al.*, Experimental evidence of radiation reaction in the collision of a high-intensity laser pulse with a laser-wakefield accelerated electron beam, Phys. Rev. X **8**, 011020 (2018).

[3] S. Kneip, C. McGuffey, F. Dollar, M. S. Bloom, V. Chvykov, G. Kalintchenko, K. Krushelnick, A. Maksimchuk, S. P. D. Mangles, T. Matsuoka, Z. Najmudin, C. A. J. Palmer, J. Schreiber, W. Schumaker, A. G. R. Thomas, and V. Yanovsky, X-ray phase contrast imaging of biological specimens with femtosecond pulses of betatron radiation from a compact laser plasma wakefield accelerator, Appl. Phys. Lett. **99**, 093701 (2011).

[4] S. P. D. Mangles, C. D. Murphy, Z. Najmudin, A. G. Thomas, J. L. Collier, A. E. Dangor, E. J. Divall, P. S. Foster, J. G. Gallacher, C. J. Hooker, D. A. Jaroszynski, A. J. Langley, W. B. Mori, P. A. Norreys, F. S. Tsung, R. Viskup, B. R. Walton, and K. Krushelnick, Monoenergetic beams of relativistic electrons from intense laser-plasma interactions, Nature (London) **431**, 535 (2004).

[5] C. G. R. Geddes, C. S. Toth, J. Van Tilborg, E. Esarey, C. B. Schroeder, D. Bruhwiler, C. Nieter, J. Cary, and W. P. Leemans, High-quality electron beams from a laser wakefield accelerator using plasma-channel guiding, Nature (London) **431**, 538 (2004).

[6] J. Faure, Y. Glinec, A. Pukhov, S. Kiselev, S. Gordienko, E. Lefebvre, J. P. Rousseau, F. Burgy, and V. Malka, A laser–plasma accelerator producing monoenergetic electron beams, Nature (London) **431**, 541 (2004).

[7] J. Couperus Cabadağ, R. Pausch, A. Köhler, O. Zarini, J. Krämer, M. Garten, A. Huebl, R. Gebhardt, U. Helbig, S. Bock, K. Zeil, A. Debus, M. Bussmann, U. Schramm, and A. Irman, Demonstration of a beam loaded nanocoulomb-class laser wakefield accelerator, Nat. Commun. **8**, 487 (2017).

[8] A. J. Gonsalves, K. Nakamura, J. Daniels, C. Benedetti, C. Pieronek, T. C. H. de Raadt, S. Steinke, J. H. Bin, S. S. Bulanov, J. van Tilborg, C. G. R. Geddes, C. B. Schroeder, C. Tóth, E. Esarey, K. Swanson, L. Fan-Chiang, G. Bagdasarov, N. Bobrova, V. Gasilov, G. Korn, P. Sasorov, and W. P. Leemans, Petawatt laser guiding and electron beam acceleration to 8 GeV in a laser-heated capillary discharge waveguide, Phys. Rev. Lett. **122**, 084801 (2019).

[9] A. D. Debus, M. Bussmann, U. Schramm, R. Sauerbrey, C. D. Murphy, Z. Major, R. Hörlein, L. Veisz, K. Schmid, J. Schreiber, K. Witte, S. P. Jamison, J. G. Gallacher, D. A. Jaroszynski, M. C. Kaluza, B. Hidding, S. Kiselev, R. Heathcote, P. S. Foster, D. Neely, E. J. Divall, C. J. Hooker, J. M. Smith, K. Ertel, A. J. Langley, P. Norreys, J. L. Collier, and S. Karsch, Electron bunch length measurements from laser-accelerated electrons using single-shot THz time-domain interferometry, Phys. Rev. Lett. **104**, 084802 (2010).

[10] O. Lundh, J. Lim, C. Rechatin, L. Ammoura, A. Ben-Ismaïl, X. Davoine, G. Gallot, J. P. Goddet, E. Lefebvre, V. Malka, and J. Faure, Few femtosecond, few kiloampere electron bunch produced by a laser-plasma accelerator, Nat. Phys. **7**, 219 (2011).

[11] G. Sarri, D. J. Corvan, W. Schumaker, J. M. Cole, A. Di Piazza, H. Ahmed, C. Harvey, C. H. Keitel, K. Krushelnick, S. P. D. Mangles, Z. Najmudin, D. Symes, A. G. R. Thomas, M. Yeung, Z. Zhao, and M. Zepf, Ultrahigh brilliance multi-MeV γ-ray beams from nonlinear relativistic Thomson scattering, Phys. Rev. Lett. **113**, 224801 (2014).

[12] Z. H. He, B. Beaurepaire, J. A. Nees, G. Gallé, S. A. Scott, J. R. S. Pérez, M. G. Lagally, K. Krushelnick, A. G. R. Thomas, and J. Faure, Capturing structural dynamics in crystalline silicon using chirped electrons from a laser wakefield accelerator, Sci. Rep. **6**, 36224 (2016).

[13] J. Wenz, S. Schleede, K. Khrennikov, M. Bech, P. Thibault, M. Heigoldt, F. Pfeiffer, and S. Karsch, Quantitative x-ray phase-contrast microtomography from a compact laser-driven betatron source., Nat. Commun. **6**, 7568 (2015).

[14] N. Powers, I. Ghebregziabher, G. Golovin, C. Liu, S. Chen, S. Banerjee, J. Zhang, and D. Umstadter, Quasi-monoenergetic and tunable x-rays from a laser-driven Compton light source, Nat. Photonics **8**, 28 (2014).

[15] W. Wang, K. Feng, K. Lintong, C. Yu, Y. Xu, R. Qi, Y. Chen, Z. Qin, Z. Zhang, M. Fang, J. Liu, K. Jiang, H. Wang, C. Wang, X. Yang, F. Wu, J. Liu, R. Li, and Z. Xu, Free-electron lasing at 27 nanometres based on a laser wakefield accelerator, Nature (London) **595**, 516 (2021).

[16] R. Assmann *et al.*, EuPRAXIA conceptual design report, Eur. Phys. J. Spec. Top. **229**, 3675 (2020).

[17] F. Albert *et al.*, 2020 roadmap on plasma accelerators, New J. Phys. **23**, 031101 (2021).

[18] J. Osterhoff, A. Popp, Z. Major, B. Marx, T. P. Rowlands-Rees, M. Fuchs, M. Geissler, R. Hörlein, B. Hidding, S.

Becker, E. A. Peralta, U. Schramm, F. Grüner, D. Habs, F. Krausz, S. M. Hooker, and S. Karsch, Generation of stable, low-divergence electron beams by laser-wakefield acceleration in a steady-state-flow gas cell, Phys. Rev. Lett. **101**, 085002 (2008).

[19] J. Vieira, S. F. Martins, F. Fiúza, C. K. Huang, W. B. Mori, S. P. D. Mangles, S. Kneip, S. Nagel, Z. Najmudin, and L. O. Silva, Influence of realistic parameters on state-of-the-art laser wakefield accelerator experiments, Plasma Phys. Controlled Fusion **54**, 055010 (2012).

[20] J. Faure, C. Rechatin, A. Norlin, A. Lifschitz, Y. Glinec, and V. Malka, Controlled injection and acceleration of electrons in plasma wakefields by colliding laser pulses, Nature (London) **444**, 737 (2006).

[21] A. Buck, J. Wenz, J. Xu, K. Khrennikov, K. Schmid, M. Heigoldt, J. M. Mikhailova, M. Geissler, B. Shen, F. Krausz, S. Karsch, and L. Veisz, Shock-front injector for high-quality laser-plasma acceleration, Phys. Rev. Lett. **110**, 185006 (2013).

[22] A. R. Maier, N. M. Delbos, T. Eichner, L. Hübner, S. Jalas, L. Jeppe, S. W. Jolly, M. Kirchen, V. Leroux, P. Messner, M. Schnepp, M. Trunk, P. A. Walker, C. Werle, and P. Winkler, Decoding sources of energy variability in a laser-plasma accelerator, Phys. Rev. X **10**, 031039 (2020).

[23] S. Bohlen, J. C. Wood, T. Brümmer, F. Grüner, C. A. Lindstrøm, M. Meisel, T. Staufer, R. D'Arcy, K. Põder, and J. Osterhoff, Stability of ionization-injection-based laser-plasma accelerators, Phys. Rev. Accel. Beams **25**, 031301 (2022).

[24] H. Suk, N. Barov, J. B. Rosenzweig, and E. Esarey, Plasma electron trapping and acceleration in a plasma wake field using a density transition, Phys. Rev. Lett. **86**, 1011 (2001).

[25] S. Bulanov, N. Naumova, F. Pegoraro, and J. Sakai, Particle injection into the wave acceleration phase due to nonlinear wake wave breaking, Phys. Rev. E **58**, R5257 (1998).

[26] K. Schmid, A. Buck, C. M. S. Sears, J. M. Mikhailova, R. Tautz, D. Herrmann, M. Geissler, F. Krausz, and L. Veisz, Density-transition based electron injector for laser driven wakefield accelerators, Phys. Rev. ST Accel. Beams **13**, 091301 (2010).

[27] K. K. Swanson, H.-E. Tsai, S. K. Barber, R. Lehe, H.-S. Mao, S. Steinke, J. van Tilborg, K. Nakamura, C. G. R. Geddes, C. B. Schroeder, E. Esarey, and W. P. Leemans, Control of tunable, monoenergetic laser-plasma-accelerated electron beams using a shock-induced density downramp injector, Phys. Rev. Accel. Beams **20**, 051301 (2017).

[28] H.-E. Tsai, K. K. Swanson, S. K. Barber, R. Lehe, H.-S. Mao, D. E. Mittelberger, S. Steinke, K. Nakamura, J. van Tilborg, C. Schroeder, E. Esarey, C. G. R. Geddes, and W. Leemans, Control of quasi-monoenergetic electron beams from laser-plasma accelerators with adjustable shock density profile, Phys. Plasmas **25**, 043107 (2018)..

[29] L. Fan-Chiang, H.-S. Mao, H.-E. Tsai, T. Ostermayr, K. K. Swanson, S. K. Barber, S. Steinke, J. van Tilborg, C. G. R. Geddes, and W. P. Leemans, Gas density structure of supersonic flows impinged on by thin blades for laser–plasma accelerator targets, Phys. Fluids **32**, 066108 (2020).

[30] S. A. Samant, A. K. Upadhyay, and S. Krishnagopal, High brightness electron beams from density transition laser wakefield acceleration for short-wavelength free-electron lasers, Plasma Phys. Controlled Fusion **56**, 095003 (2014).

[31] H. Ekerfelt, M. Hansson, I. Gallardo González, X. Davoine, and O. Lundh, A tunable electron beam source using trapping of electrons in a density down-ramp in laser wakefield acceleration, Sci. Rep. **7**, 12229 (2017).

[32] F. Massimo, A. F. Lifschitz, C. Thaury, and V. Malka, Numerical studies of density transition injection in laser wakefield acceleration, Plasma Phys. Controlled Fusion **59**, 085004 (2017).

[33] F. Massimo, A. F. Lifschitz, C. Thaury, and V. Malka, Numerical study of laser energy effects on density transition injection in laser wakefield acceleration, Plasma Phys. Controlled Fusion **60**, 034005 (2018).

[34] M. J. V. Streeter, C. Colgan, C. C. Cobo, C. Arran, E. E. Los, R. Watt, N. Bourgeois, L. Calvin, J. Carderelli, N. Cavanagh *et al.*, Laser wakefield accelerator modelling with variational neural networks, High Power Laser Sci. Eng. **11**, 1 (2023).

[35] T. D. Arber, K. Bennett, C. S. Brady, A. Lawrence-Douglas, M. G. Ramsay, N. J. Sircombe, P. Gillies, R. G. Evans, H. Schmitz, A. R. Bell, and C. P. Ridgers, Contemporary particle-in-cell approach to laser-plasma modelling, Plasma Phys. Controlled Fusion **57**, 113001 (2015).